Polymer Vol. 39 No. 16, pp. 3611–3621, 1998

0032-3861/98/$19.00+0.00

PII: S0032-3861(97)10127-6

Confirmation of predicted polymer blend morphologies from bulk specimens

Timothy J. Cavanaugh[a], K. Buttle[b], J. N. Turner[b] and E. Bruce Nauman[a,*]
[a]*The Isermann Department of Chemical Engineering, Rensselaer Polytechnic Institute, Troy, NY 12180-3590 USA*
[b]*Wadsworth Center, New York State Department of Health, Albany, NY 12221, USA*
(Received 3 July 1997; revised 18 September 1997)

The morphologies of polymer blends predicted by simulation of spinodal decomposition were compared to bulk blends made by compositional quenching. After selective staining with ruthenium and osmium tetroxide, the experimental blends were investigated microscopically using a 1.2 MeV electron microscope. Due to the penetration power of megavolt electrons, thick specimens, 0.75 μm, were examined and allowed the blend structures to be studied in all three spatial dimensions. The simulation model was successful in the prediction of the gross morphology but did not predict details such as micelle formation. With the model, it is possible to produce a desired morphology with a minimal amount of experimentation. © 1998 Elsevier Science Ltd. All rights reserved.

(Keywords: polymer blends; morphology; spinodal decomposition)

INTRODUCTION

Polymer blending has been an area of great interest over the past several decades. Blending offers the advantage of producing a material with desired properties, such as toughness or processability, without the expensive cost of developing a new monomer or a new polymerization method. The most common examples involve the impact modification of a thermoplastic, such as poly(vinyl chloride) (PVC), by the microdispersion of a rubber, such as nitrile rubber (NBR), into the matrix[1].

The blending of two immiscible polymers rarely results in a material with favourable properties. The polymers typically segregate into macroscopic domains that have high interfacial tension and poor interfacial adhesion. The resulting material will have poor mechanical properties. To improve mechanical properties, researchers have focused much of their attention on the use of interfacial agents and on the production of three desired morphologies: core-shell, cocontinuous, and dual discrete particle.

Because of its success in improving blend properties, typically impact strength, the core-shell morphology has been the subject of much investigation. In principle, the rubbery core provides resistance to impact while the glassy shell contributes compatibility with the matrix. One approach to producing this morphology involves the addition of a third component, typically a block or graft copolymer[2]. The copolymer migrates to the interface and can improve mechanical properties of the blend by decreasing interfacial tension and enhancing interfacial adhesion between the phases[3–12]. The use of impact modifiers of the core–shell type has improved the impact strength of poly(butylene terephthalate) (PBT)[13–16], polycarbonate (PC)[13,14] and epoxies[17,18].

The cocontinuous structure has rarely been observed for systems undergoing bulk spinodal decomposition. The destruction of the cocontinuity is due to hydrodynamic instabilities[19–21]. Most experimental reports of cocontinuity involve solution blends cast into thin films[22–26], where hydrodynamics are negligible. Dalknoki-Veress *et al.*[22] examined the morphology of phase separation of PS and polyisoprene (PI) on various substrates. They found large differences between the morphologies of similar blend compositions on different substrates. A few cocontinuous structures have been obtained from melt blending. Fayt *et al.*[27–29] produced a bulk cocontinuous structure when blending 20 wt% low-density polyethylene (LDPE) with 80 wt% PS on a two-roll mill. However, the structure was unstable with time and broke down into LDPE particles in the polystyrene (PS) matrix. The structure was stabilized by the addition of a tapered, hydrogenated PS/polybutadiene (PB) block copolymer[30].

The effectiveness of the dual discrete particle morphology in improving polymer blend properties has been the focus of some debate. For polymers such as acrylonitrile–butadiene–styrene (ABS) that fail by both crazing and shear yielding, it is believed that a bimodal distribution of rubber particle sizes enhances toughness compared to the same material with only one particle size population[31]. Even for polymers which fail by crazing alone, such as PS, there has been some evidence that a dual particle size morphology is effective in increasing toughness[32,33]. However, all published results involved occluded matrix particles in the larger, grafted rubber particles. It is postulated that the increase in toughness is due to the increase in volume fraction of the dispersed phase and not the bimodal particle size distribution[31].

With an ever-increasing need for new commercial materials, researchers have expanded their focus to include materials with more than two coexisting phases[34–36]. Hobbs *et al.*[34] examined various blends of poly(methyl methacrylate) (PMMA), poly(styrene-*co*-acrylonitrile) (SAN), PBT, PC and PS. They compared their observations to predicted trends that were based on interfacial tension. They

* To whom correspondence should be addressed

modified Harkin's equation[37], which describes the tendency of a liquid to spread on a solid or another liquid, in terms of two dissimilar phases dispersed in a third phase. Their blends showed reasonable agreement with the predictions. The study by Guo *et al*.[35] on ternary blends of high-density polyethylene (HDPE)/PMMA/PS and HDPE/PP/PS showed the importance of phase morphologies on mechanical properties of polymer blends. Guo et al.[36] developed a model, based on interfacial free energy, to postulate morphologies of the two dispersed phases. The interfacial free energies of the system were calculated from interfacial tensions and interfacial areas. They speculated that the interfacial tension plays a major role in establishing phase structure while the surface area of the dispersed phases has a less significant role. Despite their successes, both models examined only morphologies where the two minor components produced discrete particles. More importantly, their models are not capable of providing any graphical displays to compare to the actual blend morphologies. Due to these inadequacies, there is a need for a competent design system for multicomponent polymer blends.

Table 1 Interaction parameters for blend systems

Blend	Calculated χ from Small[45]	Simulated $n\chi$ value
	χ_{AB},χ_{AC},χ_{BC}	χ_{AB},χ_{AC},χ_{BC}
PS/PB	0.094	7.5
PS/PB/Block 730A	0.094, 0.031, 0.017	7.5, 4.0, 3.1
PS/PB/Block S142	0.094, 0.015, 0.043	7.5, 3.0, 4.5
PS/PB/PP	0.094, 0.134, 0.014	7.5, 10.0, 3.0
PS/PMMA/PB	0.019, 0.094, 0.175	3.2, 7.5, 12.0
PS/PB/R7627	0.094, 0.027, 0.023	7.5, 3.7, 3.4

Nauman and He[38] presented a wealth of testable morphologies created by modelling spinodal decomposition without hydrodynamics in ternary polymer systems. They solved the component continuity equations, which are fourth-order partial differential equations, by using a finite difference approach. Despite the mathematical complexity of the equations, there are only a few adjustable parameters: the chain lengths of the polymers, their interaction parameters and the volume fractions. The simulations,

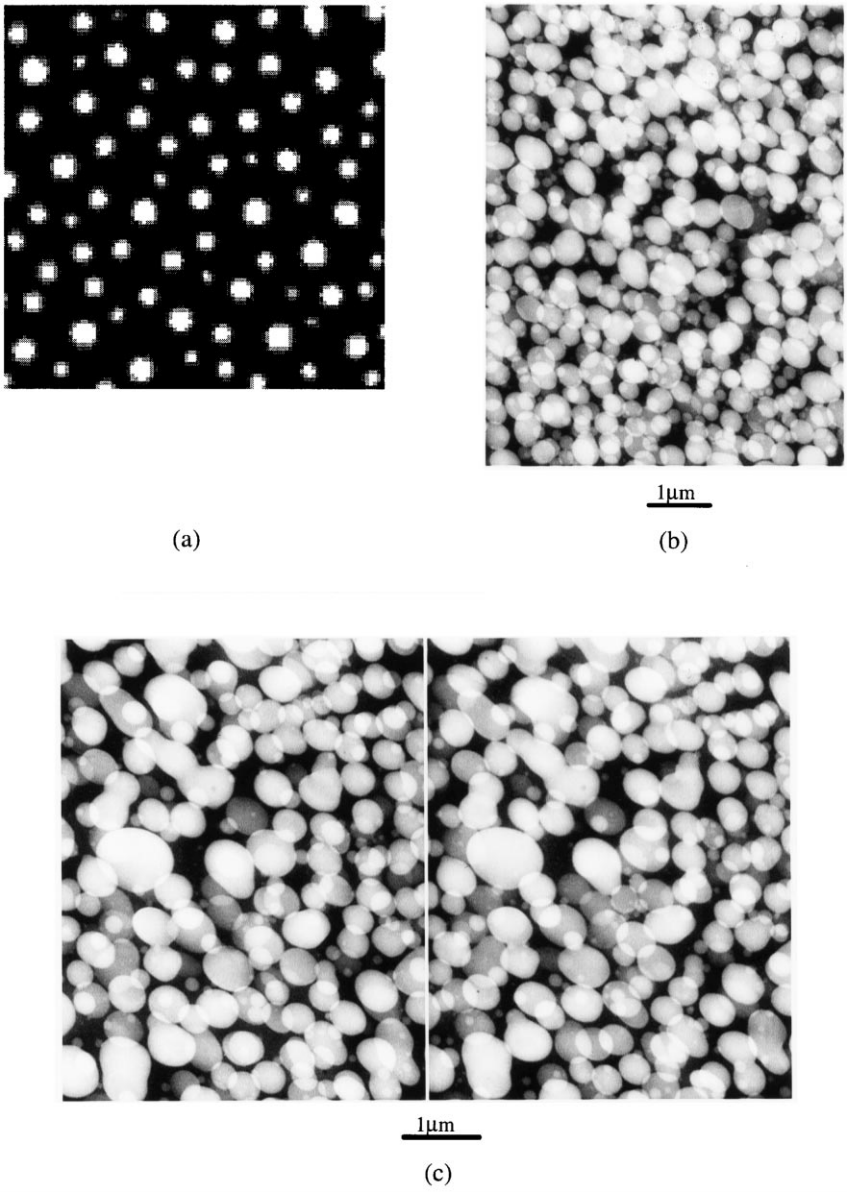

Figure 1 Comparison of (a) simulation, (b) an HVEM micrograph of a 0.75 μm section and (c) a stereopair of a bulk blend of PB/PB/730A (74.6/17.4/8) tilted at $\pm$ 8°

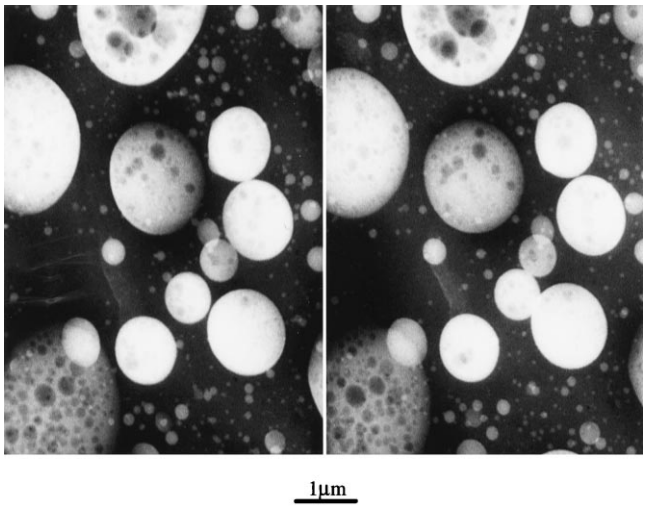

Figure 2 Stereo HVEM micrograph, recorded at ± 8°, of the excess diblock of PS/PB/730A (74.6/17.4/8) appearing as micelles

performed in two spatial dimensions, began with conditions corresponding to a nearly homogeneous mixture and concluded with the calculated morphologies corresponded to a nominal time of 16 s[38].

For this model, hydrodynamics have been ignored. However, Vasishta and Nauman[21] have modeled spinodal decomposition with hydrodynamics for a binary system. They used a volumetric body force that induced convective flows during the phase separation process. The convective flows destroyed the cocontinuous structure, and discrete domains were formed.

The ternary model of Nauman and He treats the block copolymer as a third component compatible with the other two incompatible homopolymers. Kwak and Nauman[39] proposed a quaternary model that treats the block copolymer as two spatially constrained homopolymers. Both models predict core–shell morphologies with the block copolymer at the interface. However, the quaternary model predicts a slower scaling exponent compared to the ternary model. Whenever the homopolymers are sufficiently incompatible, the quaternary model may be capable of predicting internal phase separation within the pure block copolymer.

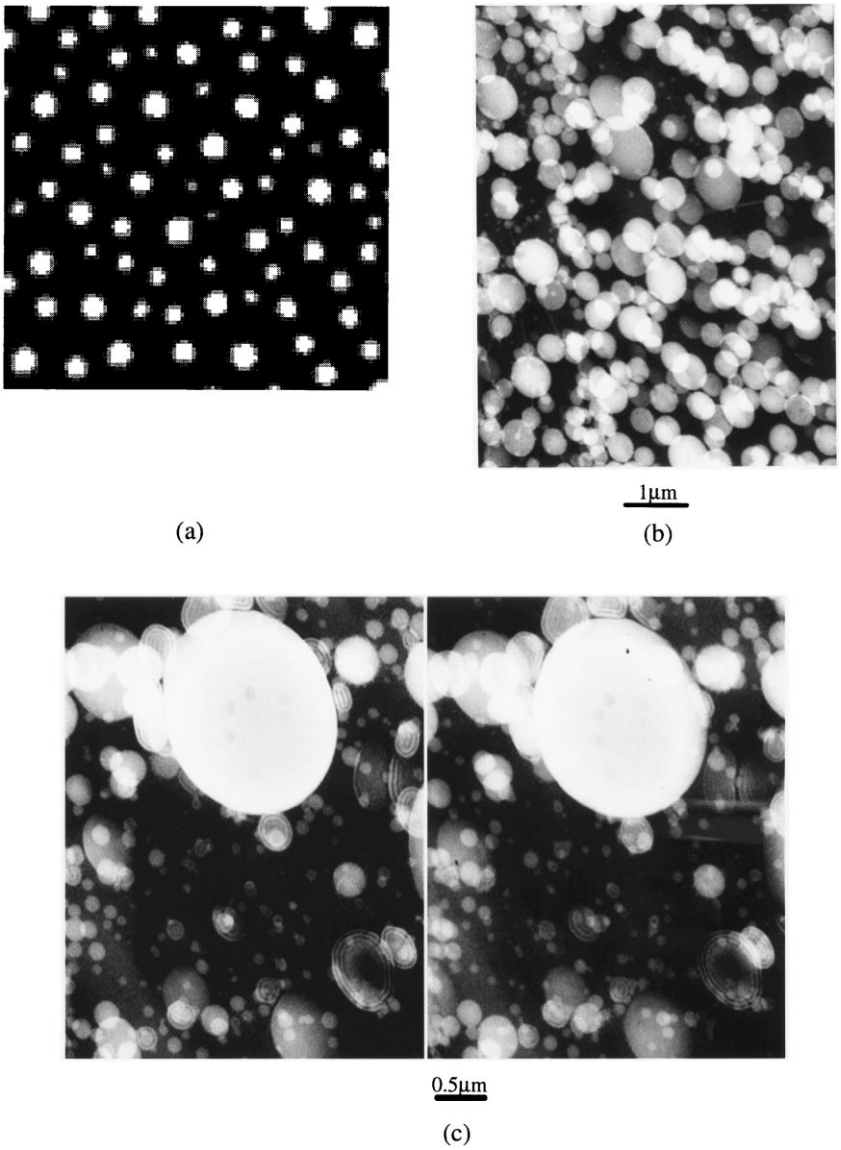

Figure 3 Comparison of (a) simulation, (b) an HVEM micrograph and (c) a stereo HVEM micrograph of PS/PB/S142 (71.4/20.6/8) recorded at ± 8°

Previously[40], we described a methodology for the design of polymer blends and gave some preliminary results for cast films and bulk samples[41]. Here we compare simulations using the Nauman and He ternary model to bulk samples produced by compositional quenching[42]. The model predicts the spatial distribution of components (morphology) and the size scale (e.g. particle size distribution). Both the model and the physical system are non-equilibrium. However, the observed morphology was quasi-stationary for most systems studied by Nauman and He. In the present study, experimental systems were chosen based on the Nauman and He predictions to generate three quasi-stationary morphologies.

The present study is restricted to morphology comparisons. However, the model also predicts a continuous increase of characteristic sizes due to Ostwald ripening and one form of coalescence. A comparison of these predictions with experimental data is given elsewhere[43].

Once the specific polymers were chosen, the interaction parameters were calculated from Hildebrand solubility parameters[44]:

$$\chi_{AB} = \left(\frac{V_r}{RT}\right)(\delta_A - \delta_B)^2 \quad (1)$$

where V_r is the reference volume, and δ_A and δ_B are the Hildebrand solubility parameters. The solubility parameters were calculated by Small's method[45]. This method was chosen for consistency. The range of literature values for χ is broad. Because of computational time limits, the interaction parameters were scaled between a maximum $n\chi$ of 12 and a minimum of 3, where n is the degree of polymerization. The minimum value of 3 was chosen to ensure phase separation in the brief simulation time. *Table 1* contains the calculated and actual $n\chi$ values used in the simulations. The various polymers are described in the experimental section. We have modeled the block and random copolymers as homopolymers. With the molecular weights known, we then chose the volume fractions to produce the specific morphology. Bulk samples were then prepared and examined using an electron microscope.

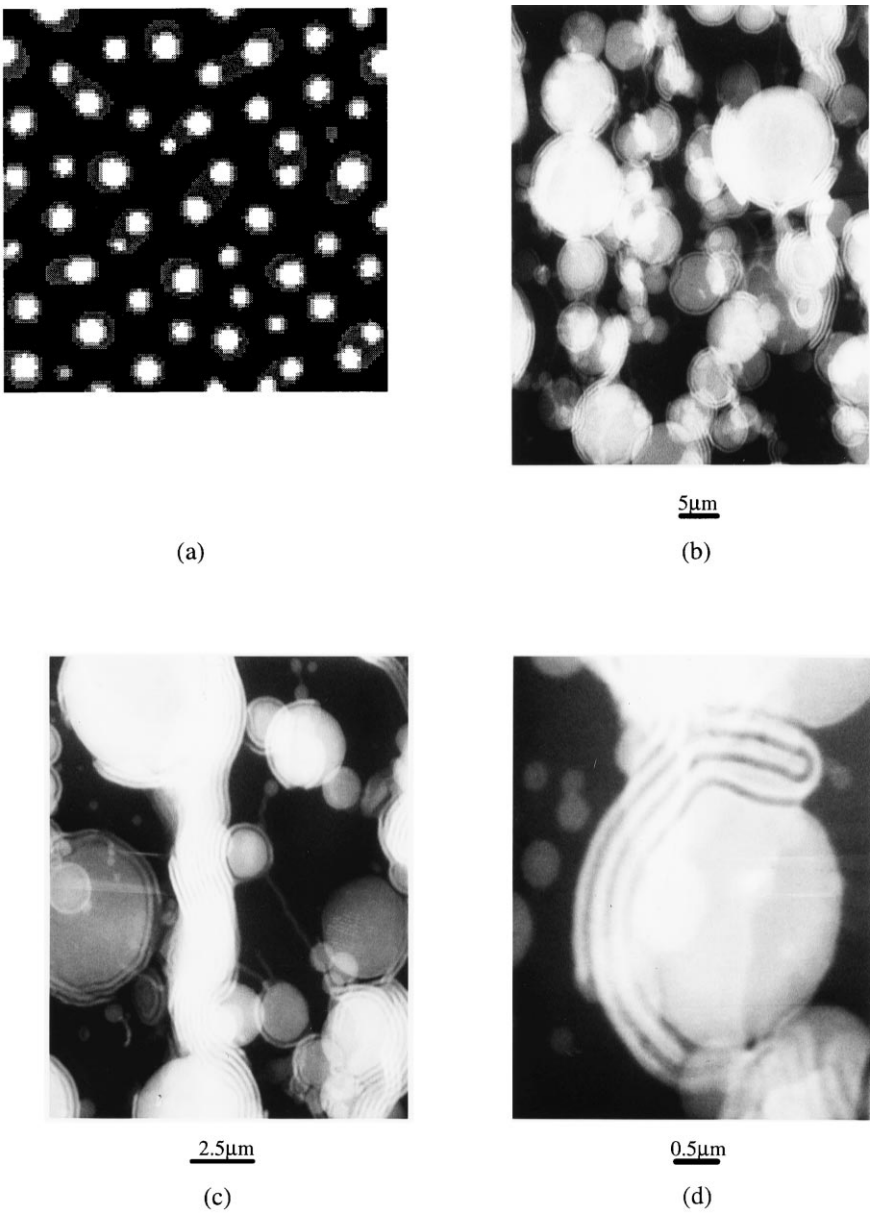

Figure 4 Comparison of (a) simulation and (b), (c) and (d) HVEM micrographs of PS/PB/S142 (64/15/21)

EXPERIMENTAL

Materials

The homopolymers and copolymers used in this study were all commercial products. A general-purpose polystyrene was obtained from Novacor Chemicals Ltd. The polybutadiene, Diene® 55NF, was acquired from Firestone. We worked with two PS/PB block copolymers, Stereon® 730A and Europrene® Sol S142. Stereon® 730A is a product of Firestone and contains 30 wt% bound PS with 23 wt% block PS. Europrene® Sol S142, which was supplied by Enichem Elastomers of America, contains 70 wt% bound PS with 46 wt% block PS. Firestone also provided a random copolymer of PS–PB, which contained 40.0% PS, called Duradene® SR7627. Escorene® (Grade 1012), an isotactic polypropylene, was obtained from Exxon Chemical. PMMA, called Plexiglass® V825, was acquired from Rohm and Haas.

Blends preparation and characterization

Homogeneous mixtures of different components and various compositions were made by dissolving the polymers in a common solvent, xylene. The total concentration of polymers was 3–5% by weight. To remove the solvent, the heated mixture was flashed into a vacuum chamber at a pressure of approximately 5 torr[42,46]. The initial polymer product contained a small amount of solvent that was removed by further devolatilization. After drying, the blend was ground into a powder and compression moulded into bars in a Carver hydraulic press at 200°C and 200 psi for various times.

The specimens containing PB, except for those containing the Duradene® SR7627 as well, were immersed for 2 weeks in a 4% aqueous solution of osmium tetroxide (OsO_4)[47]. The sections were cut to approximately 0.75 μm in thickness using a Reichert–Jung Ultracut E ultramicrotome with a diamond knife. Sections containing PMMA were stained further with ruthenium tetroxide (RuO_4) vapour for 3 min to provide more contrast[48]. Samples containing Duradene® SR7627 were cryomicrotomed, at a temperature of −120°C, to a thickness of 0.75 μm using an RMC CR-X cryoultramicrotome. These sections were then stained with OsO_4 vapour for 3 min. The morphologies were examined using an AEI Mark IV high voltage electron microscope (HVEM) at 1.2 MeV. Using a tilt rotation stage[49], stereo pairs were recorded, to provide direct three-dimensional (3-D) viewing. The specimens were tilted, and two images of the same field from different perspectives,

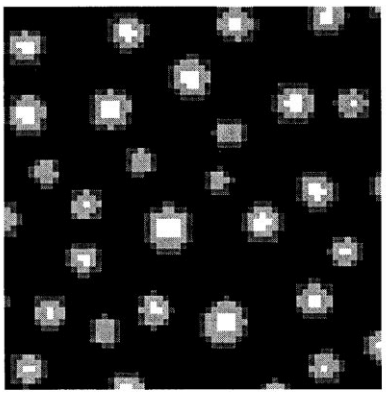

(a)

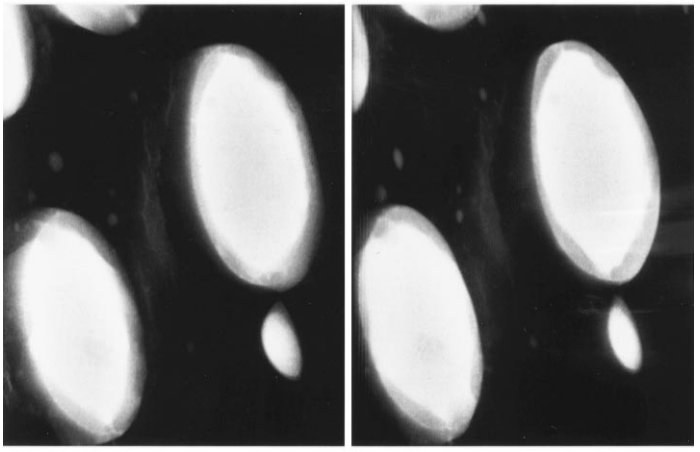

1μm

(b)

Figure 5 Comparison of (a) simulation and (b) an HVEM micrograph, recorded at ± 8°, of PS/PB/SR7627 (74/18/8)

i.e. different orientations relative to the optical axis of the microscope, were recorded. When oriented and viewed appropriately[49], the angular separation produces left–right parallax which allows direct 3-D viewing of thick specimens. The stereo effect is visualized when the viewer fuses two images by crossing their eyes. The viewer concentrates on a particular feature and makes the two images overlap. This helps fuse the stereo image. All negatives from the electron microscope were digitized and processed to produce photographic quality images.

RESULTS AND DISCUSSION

Core-shell structure

PS/PB/diblock (PS–PB). *Figure 1a* is a simulation of a blend of PS/PB/730A (74.6/17.4/8.0). The diblock appears as the grey ring around the spheres of PB. The corresponding HVEM micrograph is shown in *Figure 1b*, which is a projection of a 0.75-μm-thick specimen. The location of the block copolymer is not obvious in this picture, but it is believed to be at the interface of the rubber particle and the matrix. Because the sections are thicker than conventional TEM samples, the particle overlap is quite extensive, and the phase volumes of the PB appear much higher than the 2-D simulation. *Figure 1c*, which is a stereopair of the blend, provides excellent 3-D details of the discrete particles in the matrix. Many of the particles are elliptically shaped, which we attribute to coalescence. Upon moulding for longer times, the particles grow, and therefore the total interfacial area decreases. The excess diblock appears as micelles in the PB phase, see *Figure 2*.

A similar blend (71.4/20.6/8), using S142 instead of 730A, is shown in *Figure 3*. At early moulding times, there appears to be no surplus diblock. At later times, the excess diblock appears as 'onion structures' in the matrix as well as a small number of micelles in the PB. The presence of the diblock in both homopolymers is attributed to the fact that the block lengths of the S142 are commensurate. It is speculated that micelles will preferentially form in the homopolymer which corresponds to the longer block length of the copolymer. As the composition of the diblock in the blend increases to 64/15/21, lamellar structures form at the interface and extend into the matrix, as seen in *Figure 4*. Our

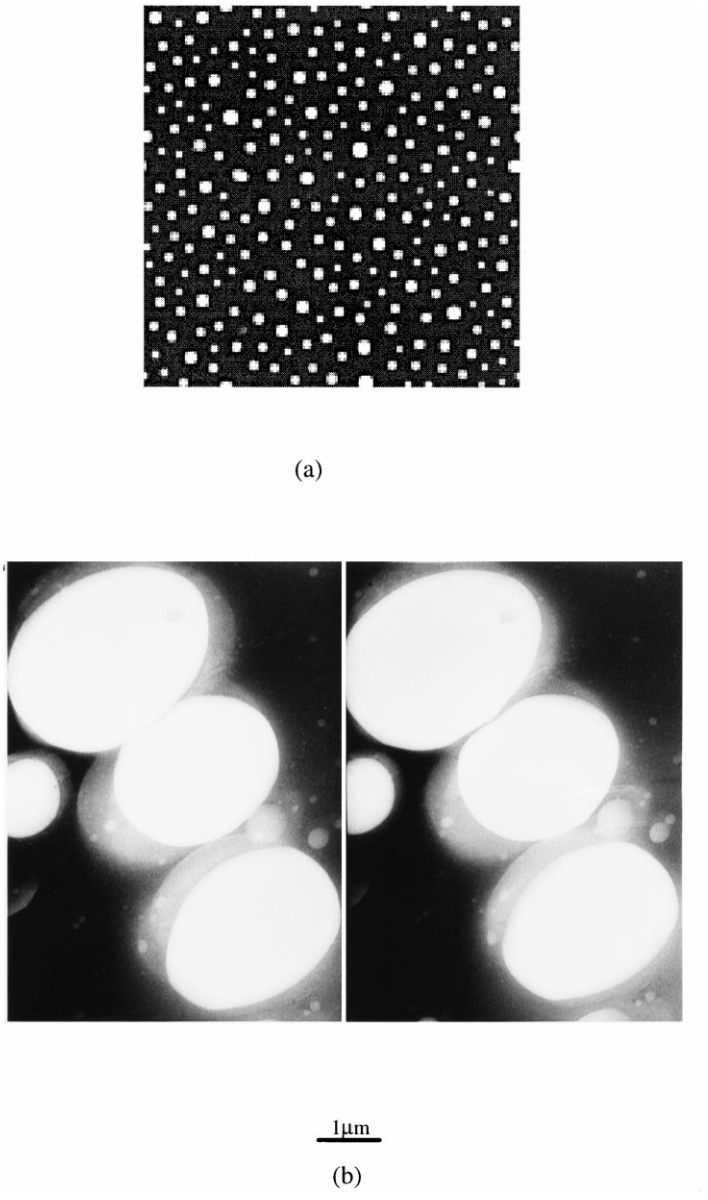

Figure 6 Comparison of (a) simulation and (b) stereopair, tilted at ± 8°, of PMMA/PS/PB (77/8/15)

simulations predict an asymmetric core–shell structure. This asymmetric core is believed to be due to the coalescing of the dispersed phase. The correction to a symmetric core–shell structure, which is the favoured free energy state, presumably occurs over long times. For this system, the model accurately predicts the macrophase separation but cannot model the microphase separation of the block copolymer.

PS/PB/random (PS–PB). As with the previous system, our model indicates that the copolymer will be at the interface of the two homopolymers, as seen in *Figure 5a*. Since the random copolymer contains approximately 40% PS, it will be less white on the negative, compared to the PB particles, after staining with the osmium tetroxide. In the stereopair, *Figure 5b*, the random copolymer appears as a light shell, which encapsulates the PB. As is the case with ternary blends containing diblock, the copolymer is not uniform around the particle. The overall prediction matches the simulation.

PMMA/PS/PB. In this ternary system (77/8/15), the model predicts that the PS, the thin black shell, will encapsulate the PB domains, as seen in *Figure 6a*. To provide more contrast between PMMA and PS, the experimental sample was stained with RuO_4. In *Figure 6b*, the unstained PMMA appears as the dark matrix, while the PS is the light shell around the PB particles. When viewed as a stereopair, the PS is seen to encapsulate the PB particles. This confirms the predicted morphology and shows that good penetration of the RuO_4 staining agent was obtained. It also appears that the PS shell is hindering coalescence of the particles.

PS/PB/PP. For the previous systems, the blends contained a rubbery core with a glassy shell. In *Figure 7* and *Figure 8*, the simulations of compositions of (77/15/8) and (77/8/15) predict that the PP will be the core, black in colour, surrounded by a shell of PB. In the case of (77/15/8), the PP was encapsulated by the PB, but the PP was close to the interface as opposed to being in the centre, see *Figure 7b*. In

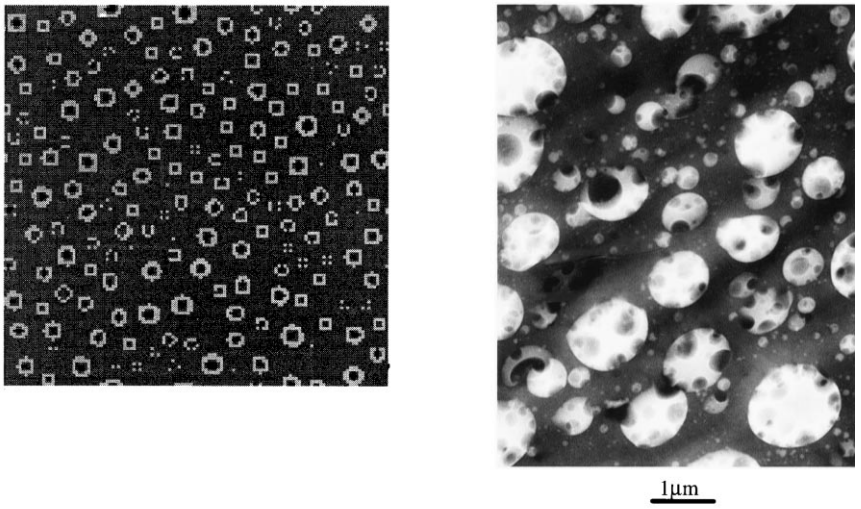

Figure 7 Comparison of (a) simulation and (b) bulk HVEM of PS/PB/PP (77/15/8)

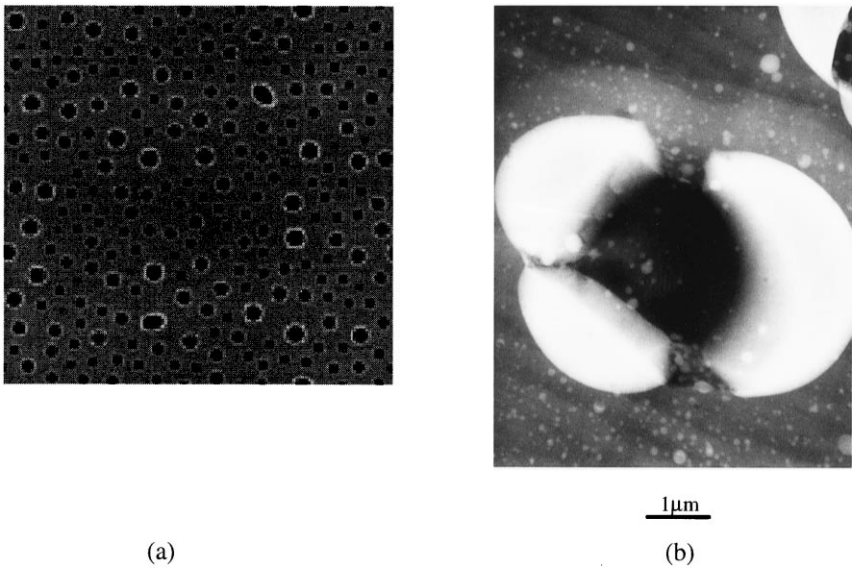

Figure 8 Comparison of (a) simulation and (b) bulk HVEM of PS/PB/PP (77/8/15)

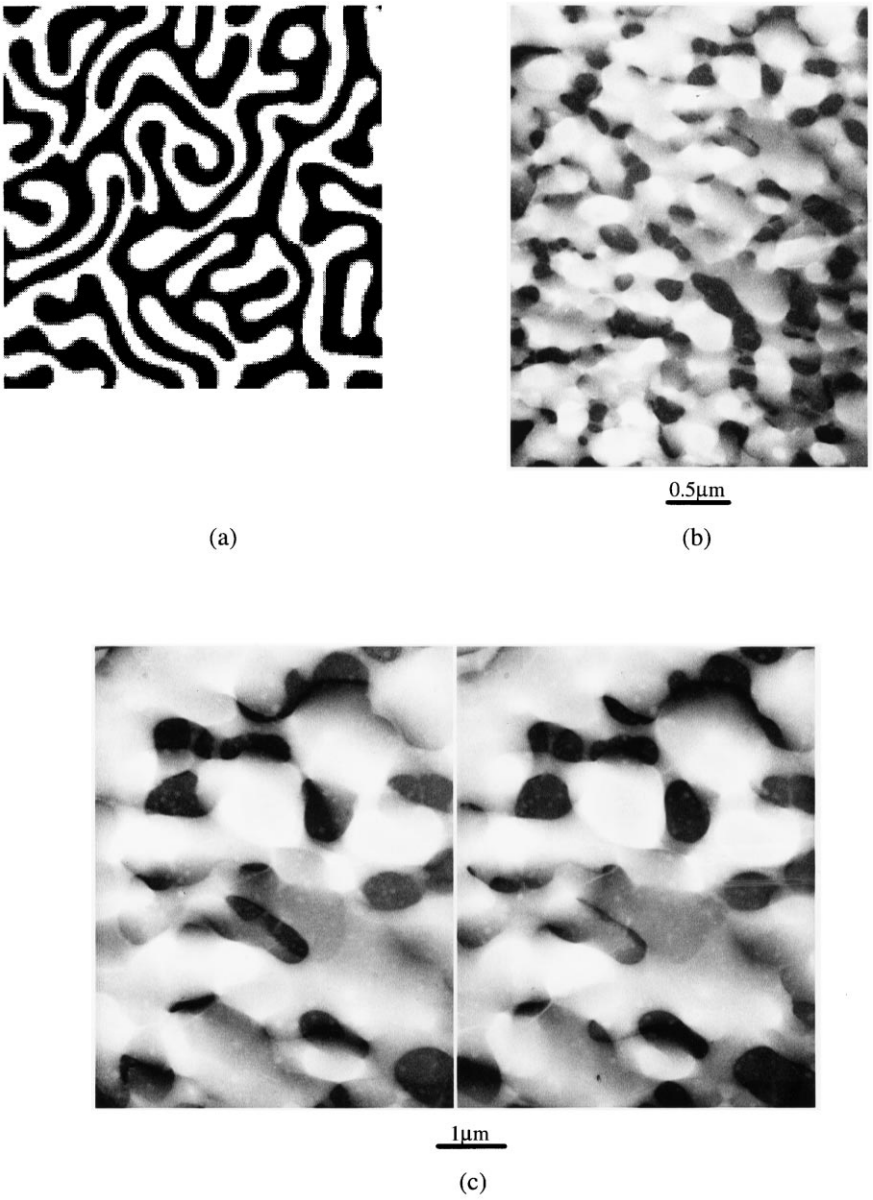

Figure 9 Comparison of (a) simulation, (b) bulk HVEM and (c) stereopair, recorded at ± 8°, of PS/PB (50/50)

the case of (77/8/15), the model and the experiment do not agree, as seen in *Figure 8*. Although there is some tendency towards envelope formation, the PB domains remain distinct but attached to the PP. The discrepancy between the simulation and experimental blends may be due to the effects of the crystallization of PP on the morphology[36].

Cocontinuous structure

Figure 9 represents the results of a critical quench (50/50) of PS/PB. The simulation predicts a dual semicontinuous structure, in 2-D, that would presumably be cocontinuous in 3-D. After examining the stereopair, *Figure 9c*, both domains appear to be cocontinuous and resemble the 3-D reconstruction from light scattering data of Jinnai *et al.*[50]. After ripening over longer periods of time, the morphology begins to break down into disperse but irregular domains of PB in PS, as shown in *Figure 10*. Since the current model does not account for hydrodynamic flows, the loss in cocontinuity is not predicted, but it is predicted by the model of Vasishta and Nauman[21].

Dual discrete particle structure

As seen in *Figure 11a*, the system of PS/PMMA/PB (77/8/15) produces particles of both PMMA and PB. The experimental blend, *Figure 11b*, shows two sets of discrete particles with the PMMA being the larger dark spheres. The simulation predicted this morphology but does not predict the much larger size of the PMMA particles. Particle size differences can be due to different initial sizes (the minimum size for growth) or different ripening rates. The ripening rate depends on solubilities and diffusivities within the continuous phase. The current model reflected the first two factors but assumed the same diffusivity for all species. The experiments suggest that the diffusivity of the PMMA in PS is much higher than that of PB in PS. This difference could be reflected in future simulations[51]. *Figure 11c* shows that at longer ripening times, the smaller PB particles are no longer uniformly distributed in the matrix but accumulate at the interface of the larger PMMA particles. The physical sample shown in *Figure 11c* was ripened for 1 hr. Our simulation, which does not show this clustering effect, was limited to a relatively short ripening time, nominally 16 s.

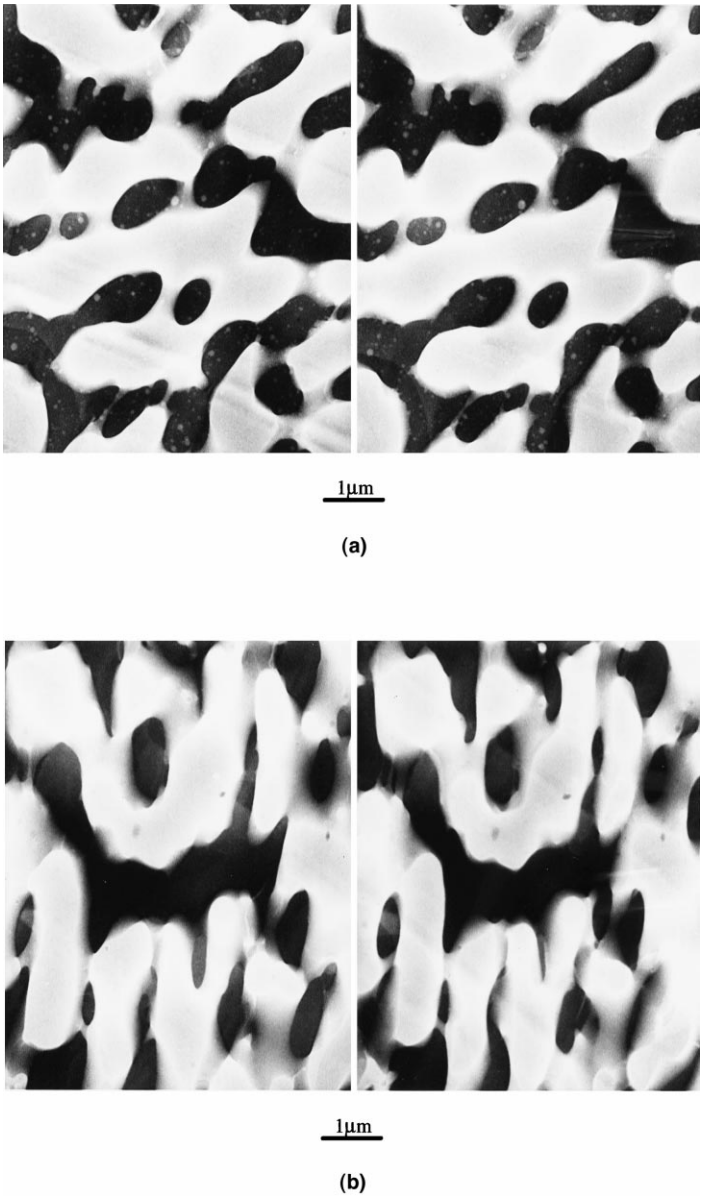

Figure 10 Stereopairs of later ripening times of PS/PB (50/50): (a) 30 min; (b) 60 min

Due to the large $n\chi$ value of 12, which is near the upper limit of the algorithm, the computational time required to predict the viewed morphology would be excessive. In an attempt to provide some understanding of the observed morphology, we performed 1-D simulations. Two discrete phases, one being PMMA and the other PB, were placed at various distances apart. The volume fractions of the phases were consistent with the 2-D simulations. In cases where the distance between the particles was non-zero, the particles were separated by a PS phase. At each distance, a scaled free energy was calculated. *Figure 12* shows that, at close distances, there is a local minimum in the free energy.

CONCLUSIONS

We have confirmed that the model of ternary polymer blends undergoing spinodal decomposition accurately predicts gross morphologies. We were able to produce a wide range of desired morphologies with a minimal amount of experimentation. Our studies demonstrate the strong dependence of phase morphology on volume fractions of the components. Also, it appears that coalescence plays an important role in phase ripening of these systems.

The use of the HVEM in the analysis of polymer blend morphologies has proven a valuable instrument. Using thick specimens, we were able to observe structures, such as the cocontinuous structure, in three spatial dimensions. The thicker specimens allowed us to obtain greater details about the morphologies and phase ripening of polymer blends. Eventually, we hope to use the HVEM to acquire more quantitative information of polymer blends, such as particle size distributions.

As expected, the model could not predict microphase separation of the block copolymers nor could it account for the effects of crystallization on phase morphology.

Despite these shortcomings, the model is an excellent tool for the design of polymer blends. The next important step is to relate blend morphology to blend property with a correlation. Once this is completed, we will have an invaluable tool with which to design multicomponent polymer blends.

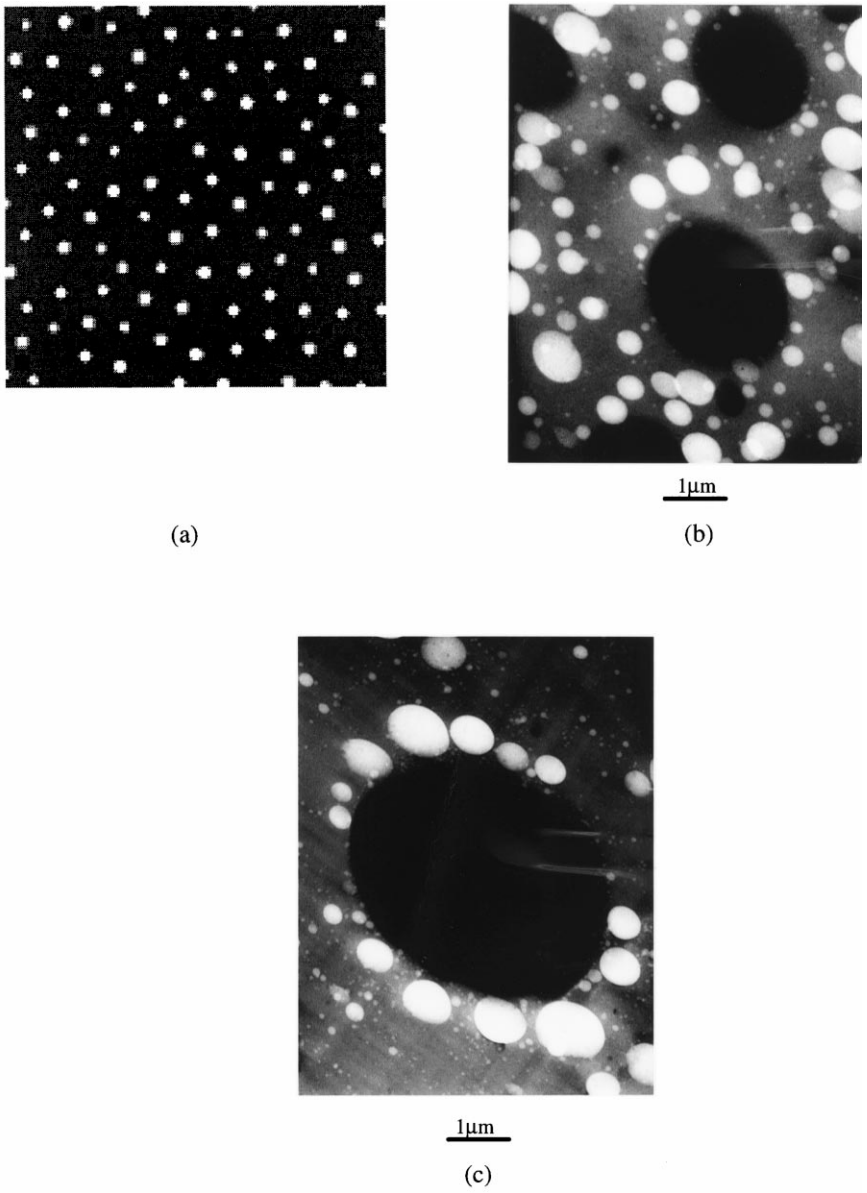

Figure 11 Comparison of (a) simulation and (b) bulk HVEM of PS/PMMA/PB (77/8/15). Later ripening morphology is shown in (c)

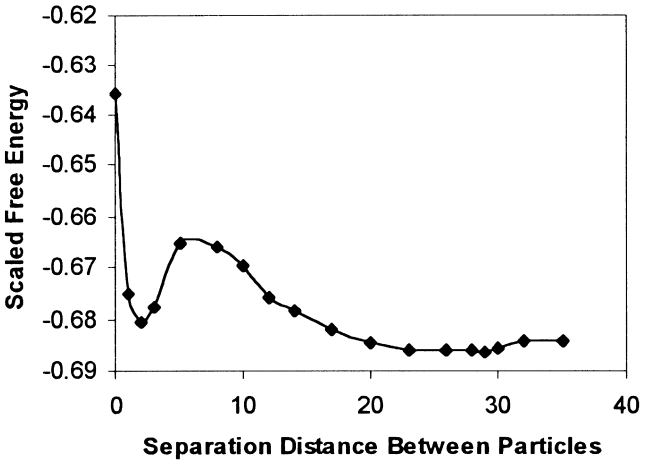

Figure 12 Free energy calculation for dual discrete particle system

ACKNOWLEDGEMENTS

The electron micrographs were obtained from the equipment that is supported in part by the Biotechnological Resource Grant RR-01219. This grant supports the Wadsworth Center's Biological Microscopy and Image Reconstruction Facility as a National Resource. The authors gratefully acknowledge the use of the cryoultramicrotome in Wadsworth's Electron Microscopy Core.Partial support of this work by the Petroleum Research Foundation, under grant #31115-AC7, is gratefully acknowledged.

REFERENCES

1. Ulrich, H. *Introduction to Industrial Polymers*, 2nd edn. Hanser, Munich, 1993.
2. Paul, D. R., in *Polymer Blends*, Vol. 2, ed. D.R. Paul and S. Newman. Academic Press, New York, 1978.
3. Shull, K. R. and Kramer, E. J., *Macromolecules*, 1990, **23**, 4769.
4. Shull, K. R., Kramer, E. J., Hadziioannou, G. and Tand, W., *Macromolecules*, 1990, **23**, 4780.
5. Brown, H. R., *Macromolecules*, 1989, **22**, 2859.
6. Fayt, R., Jerome, R. and Teyssie, Ph., *J. Polym. Sci., Polym. Phys. Ed.*, 1989, **27**, 775.

7. Brown, H. R., *Macromolecules*, 1991, **24**, 2752.
8. Creton, C., Kramer, E.J., Hoi, C. Y. and Brown, H. R., *Macromolecules*, 1992, **25**, 3075.
9. Creton, C., Kramer, E. J. and Hadziioannou, G., *Macromolecules*, 1991, **24**, 1848.
10. Anastasiadas, S., Gancarz, I. and Koberstein, J., *Macromolecules*, 1989, **22**, 1449.
11. Russell, T. P., Anastasiadas, S., Menelle, A., Felcher, G. P. and Satija, S. K., *Macromolecules*, 1991, **24**, 1575.
12. Adedeji, A. and Jamieson, A. M., *Polymer*, 1993, **34**, 5038.
13. Hobbs, S. Y., Dekkers, M. E. J. and Watkins, V. H., *J. Mater. Sci.*, 1988, **23**, 1219.
14. Hobbs, S. Y., Dekkers, M. E. J. and Watkins, V. H., *J. Mater. Sci.*, 1988, **23**, 1225.
15. Cheng, C., Hiltner, A., Baer, E., Suskey, P. R. and Mylonakis, S. G., *J. Mater. Sci.*, 1995, **30**, 587.
16. Cheng, C., Peduto, N., Hiltner, A., Baer, E., Suskey, P. R. and Mylonakis, S. G., *J. Appl. Polym. Sci.*, 1994, **53**, 513.
17. Sue, H. J., *J Mater. Sci*., 1992, **27**, 3098.
18. Sue, H. J., Bertram, J. L., Garcia-Meitin, E. I., Wilchester, J. W. and Walker, L. L., *Colloid Polym. Sci.*, 1994, **272**, 456.
19. Siggia, E. D., *Phys. Rev. A*, 1979, **20**(2), 595.
20. Rousar, I. and Nauman, E. B., *Chem. Eng. Commun*., 1991, **105**, 77.
21. Vasishta, N. and Nauman, E. B., *Proc. Am. Chem. Soc. Div. Polym. Mater*., 1993, **69**, 168.
22. Dalnoki-Veress, K., Forrest, J. A., Stevens, J. R. and Dutcher, J. R., *J. Polym. Sci. B, Polym. Phys.*, 1996, **34**, 3017.
23. Tanaka, H., Yokokawa, T., Abe, H., Takafumi, H. and Nishi, T., *Phys. Rev. Lett.*, 1990, **65**(25), 3136.
24. Okada, M., Kwak, K. D., Chiba, T. and Nose, T., *Macromolecules*, 1993, **26**, 6681.
25. Lauger, J., Lay, R., Maas, S. and Gronski, W., *Macromolecules*, 1995, **28**, 7010.
26. Inoue, T., Ougizawa, T., Yasuda, O. and Miyasaka, K., *Macromolecules*, 1985, **18**, 57.
27. Fayt, R., Jerome, R. and Teyssie, Ph., *J. Polym. Sci., Polym. Lett. Ed.*, 1981, **19**, 79.
28. Fayt, R., Jerome, R. and Teyssie, Ph., *J. Polym. Sci., Polym. Phys. Ed.*, 1981, **19**, 1269.
29. Fayt, R., Jerome, R. and Teyssie, Ph., *J. Polym. Sci., Polym. Phys. Ed.*, 1982, **20**, 2209.
30. Harrats, C., Blancher, S., Fayt, R., Jerome, R. and Teyssie, Ph., *J. Polym. Sci., Polym. Phys. Ed.*, 1995, **33**, 801.
31. Lee, W. H., in *Polymer Blends and Alloys*, ed. M. J. Folkes and P. S. Hope. Blackie Academic and Professional, London 1993.
32. Hobbs, S. Y., *Polym. Eng. Sci.*, 1986, **26**, 74.
33. Keskkula, H., Paul, D. R., McCreedy, K. M. and Henton, D. E., *Polymer*, 1987, **28**, 2063.
34. Hobbs, S. Y., Dekkers, M. E. J. and Watkins, V. H., *Polymer*, 1988, **29**, 1598.
35. Guo, H. F., Gvozdic, N. V. and Meier, D. J., *PMSE Preprint*, 1996, **75**, 444.
36. Guo, H. F., Packirisamy, S., Gvozdic, N. V. and Meier, D. J., *Polymer*, 1997, **38**, 785.
37. Harkins, W. D., *The Physical Chemistry of Surface Films*. Reinhold, New York, 1952.
38. Nauman, E. B. and He, D. Q., *Polymer*, 1994, **35**, 2243.
39. Kwak, S. and Nauman, E. B., *J. Polym. Phys., Polym. Phys. Ed.*, 1996, **34**, 1715.
40. Cavanaugh, T. J., Russo, A. P. and Nauman, E. B., *CHEMTECH*, 1996, **26**(8), 32.
41. Brunswick, A., Cavanaugh, T. J, Mathur, D., Russo, A. P. and Nauman, E. B., *J. Appl. Polym. Sci.*, 1998, **68**, 339.
42. Nauman, E. B., Ariyapadi, M. V., Balsara, N. P., Grocela, T. A., Furno, J. S., Lui, S. H. and Millikarjun, R., *Chem. Eng. Commun.*, 1988, **66**, 29.
43. Cavanaugh, T. J. and Nauman, E. B., in press.
44. Hildebrand, J. H. and Scott, R. L., *Regular Solutions*. Prentice Hall, Englewood Cliffs, New Jersey, 1962.
45. Small, P. A., *J. Appl. Chem.*, 1953, **3**, 71.
46. Nauman, E. B., in *Concise Encyclopedia of Polymer Science and Engineering*, ed. H. F. Mark. Wiley, New York, 1990.
47. Kato, K., *J. Electron Microscopy*, 1965, **14**, 219.
48. Trent, J. S., Scheinbeim, J. I. and Couchman, P. R., *Macromolecules*, 1983, **16**, 589.
49. Turner, J. N., in *Methods in Cell Biology*, Vol. 22, *Three-Dimensional Ultrastructure in Biology*, ed. J. N. Turner. Academic Press, New York, 1981.
50. Jinnai, H., Hashimoto, T., Lee, D. and Chen, S. H., *Macromolecules*, 1997, **30**, 130.
51. He, D. Q. and Nauman, E. B., *J. Polym. Sci., Polym. Phys. Ed.*, 1997, **35**, 897.